Efficient yet Accurate Solution of the Linear Transport Equation in the Presence of Internal Sources: The Exponential-Linear-in-Depth Approximation

ARVE KYLLING AND KNUT STAMNES

Geophysical Institute and Department of Physics, University of Alaska-Fairbanks, Fairbanks, Alaska 99775-0800

We present solutions to the linear transport equation valid for monoenergetic particles interacting with a multiple scattering and absorbing layered medium possessing a general anisotropic internal source term. A new exponential-linear approximation to the internal source as a function of scattering depth is introduced and compared to approximations that vary linearly and quadratically in scattering depth. The prime merit of this new approximation is to provide a very efficient yet accurate solution to the linear transport equation by substantially reducing the spatial mesh size. Numerical results pertaining to (1) an embedded thermal source and (2) a rapidly varying beam pseudo-source demonstrate that the exponential-linear approximation is vastly superior both in speed and accuracy to a linear or quadratic approximation. Potential applications include neutral (photon, neutron) or charged (electron, ion) particle transport as well as linearized gas dynamics. © 1992 Academic Press, Inc.

1. INTRODUCTION

Problems involving neutral or charged particle transport in a background medium and rarefied gas dynamics frequently require solutions of a linear transport equation derivable from the Boltzmann equation. Efficient techniques for solving the homogeneous version of this equation in slab geometry are discussed elsewhere. Here we focus on obtaining a reliable, efficient, and accurate particular solution in the presence of a general internal source term. In a variety of particle transport problems the particle distribution function $f(\mathbf{r}, \mathbf{p}, t)$ varies with location ($\mathbf{r}$), momentum ($\mathbf{p}$) and time (t). For sufficiently dilute gases the temporal and spatial evolution of the particle distribution function is described by the Boltzmann equation:

$$\frac{\partial f}{\partial t} + \nabla_r(f\mathbf{v}) + \nabla_p(f\mathbf{F}) = \tilde{Q}(\mathbf{r}, \mathbf{p}, t), \qquad (1)$$

where ∇_r and ∇_p are the gradient operators in configuration and momentum space, respectively. The particles may be subject to an external force $\mathbf{F}(\mathbf{r}, \mathbf{p}, t)$ and $\tilde{Q}(\mathbf{r}, \mathbf{p}, t)$

represents the net source due to collisions and "true" production. The Boltzmann equation is generally non-linear; however, a large class of problems exists for which a linear transport equation derivable from (1) provides an adequate physical description. Such problems include neutral (photon, neutron) or charged (electron, ion) particle interaction with a background medium (the "test-particle problem") as well as linearized gas dynamics, cf., e.g., [1–9].

Depending on the physical problem of interest, different assumptions and approximations are invoked to derive a linear version of (1) and subsequently cast it into a form amenable to solution. Numerous numerical methods exist for solving the resulting integro-differential equation. Such methods usually invoke some discretization of space, momentum, and time. This discretization will give the source term an artificial step-function behavior that may introduce errors in the computed particle distribution function if the variation in the source term within one space, momentum, or time-step is not properly accounted for.

The accuracy of a purely numerical solution to the linear transport equation is generally expected to improve with the number of mesh points used to represent the independent variables while the computer time will generally increase. However, a "brute force" discretization of the transport equation may lead to a very large system of equations, which makes a solution impractical even on modern computers. For example, in the one-dimensional slab problem, a mesh size of 100 space points, 100 energy points, and 10 angle points may be required to achieve the desired accuracy, but then a set of 10^5 simultaneous algebraic equations would have to be solved for each time step. Thus although it is usually desirable to achieve both high accuracy and high computational speed these two goals may seem to be mutually exclusive or incompatible. In view of this we may state that the general aim of this paper is to use a combination of analytical and numerical techniques to arrive at a solution to the linear transport equation in the

presence of embedded sources that requires a minimum of spatial mesh points and is both accurate and computationally efficient.

In the following we consider the steady state, linear transport equation valid for a general anisotropic source of particles embedded in a plane parallel medium represented by a horizontal slab so that spatial variation occurs only in the vertical direction. To account for the vertical inhomogeneity of the medium as well as the spatial variation of the internal source it is common to divide the slab into a number of layers. This number should be large enough that each of these layers is homogeneous in the sense that the scattering/absorption coefficients may be regarded as constant within the layer. Then the accuracy of the solution depends mainly on how well the spatial variation of the internal source across each layer is approximated.

To quantify the errors incurred by invoking different schemes of approximation, we present numerical results pertaining to radiation transport for thermal emission of radiation in a scattering and absorbing layered medium. This choice is motivated by the following observations:

1. The source is given by the Planck function which has an analytical form that is easy to work with, and the spatial variation is determined by simply specifying the temperature gradient across the slab.

2. Evaluation of the Planck function in different spectral regions provides a source term that varies both slowly and rapidly in space. Thus for $h v \ll kT$ (Rayleigh–Jeans limit) the Planck function becomes

$$B_v(T) = \frac{2v^2 kT}{c^2}, \tag{2}$$

while for $h v \gg kT$ (Wien limit), we have

$$\int B_v(T)\, dv = \frac{2h}{c^2} \int v^3 e^{-hv/kT}\, dv \approx \frac{2hv^3}{c^2} kTe^{-hv/kT} + \text{const}, \tag{3}$$

and integrated over the whole spectrum, we have the Stefan–Boltzmann law

$$B(T) = \sigma T^4. \tag{4}$$

Here σ is the Stefan–Boltzmann constant, k is the Boltzmann constant, h is the Planck constant, and c is the speed of light. Furthermore, T is the temperature and v the frequency. Assuming that the temperature T varies linearly with τ we thus have an internal source that, depending on the spectral region in question, exhibit very different behavior, e.g., linear with τ in the Rayleigh–Jeans limit, as a fourth-order polynomial in τ for the Stefan–Boltzmann law, and exponential-linear in τ in the Wien limit.

3. We expect the numerical examples to provide a good indication of the general validity and performance of the various approximation methods to be tested.

The Planck function yields an isotropic internal source. To investigate how the different approximations work for anisotropic sources we present results for a rapidly varying beam pseudo-source in a scattering and absorbing medium.

An efficient and common way of solving energy or velocity dependent linear transport problems is based on the so-called multi-group procedure in which the integration over energy (or momentum) is reduced to solving a series of monoenergetic (or one group) problems [5]. The form of the equation is identical for the various energies; the difference lies essentially in the source term representing the action of collisions and "true" embedded sources. Thus it suffices to focus on the monoenergetic equation below.

2. LINEAR TRANSPORT IN MULTIPLE SCATTERING AND ABSORBING MEDIA WITH EMBEDDED SOURCES

In a steady-state situation with no external forces the transport equation for monoenergetic particles in a plane parallel medium can be written in the form, e.g. [5, 19],

$$\mu \frac{du(\tau, \mu, \phi)}{d\tau} = u(\tau, \mu, \phi) - \frac{\omega(\tau)}{4\pi} \int_0^{2\pi} d\phi'$$

$$\times \int_{-1}^1 d\mu'\, P(\tau, \mu, \phi; \mu', \phi')\, u(\tau, \mu', \phi')$$

$$- Q(\tau, \mu, \phi), \tag{5}$$

where completely incoherent scattering is assumed. Here $u(\tau, \mu, \phi)$ is the intensity of particles at scattering depth τ moving in the direction ϕ (azimuthal angle) and μ, where μ is the cosine of the polar angle ($\mu = \cos \theta$); $\omega(\tau)$ is the single scattering albedo, $P(\tau, \mu, \phi; \mu', \phi')$ is the phase function, and $Q(\tau, \mu, \phi)$ is the gain due to collisions resulting in an energy change and "true" production, hereafter referred to simply as the source term. The first term on the right side is due to particle extinction while the second integral term is due to multiple angular scattering (no change in energy). The azimuthal dependence is usually forced upon us by an incident monodirectional beam. It can be dealt with efficiently by expanding the intensity in a Fourier cosine series as explained in Refs. [3, 10]. This leads to a series of independent equations, one for each Fourier component, but all of a form identical to the azimuthally averaged version of Eq. (5). Thus, below we will consider only the azimuthally averaged equation.

Using the discrete-ordinate method as outlined in [10], the azimuthally averaged version of the integro-differential

equation (5), is approximated by a system of $2N$ coupled ordinary differential equations,

$$\mu_i \frac{du(\tau, \mu_i)}{d\tau} = u(\tau, \mu_i) - \sum_{\substack{j=-N \\ j \neq 0}}^{N} w_j D(\tau, \mu_i, \mu_j) u(\tau, \mu_j)$$

$$- Q(\tau, \mu_i), \qquad i = \pm 1, \pm 2, ..., \pm N, \qquad (6)$$

where w_j is the quadrature weight and the coefficient $D(\tau, \mu_i, \mu_j)$ depends on the phase function and the single scattering albedo. The solution of the homogeneous version of Eq. (6) has been presented and discussed in detail elsewhere [10] and needs no further elaboration. Here we focus on finding an accurate, reliable, and efficient particular solution.

To allow for a source term that may exhibit both rapid and slow variation with τ (exemplified by the Planck function as discussed in the introduction) we approximate the source term by an exponential-polynomial function

$$Q(\tau, \mu) = e^{-\alpha\tau} \sum_{l=0}^{K} X_l(\mu) \tau^l. \qquad (7)$$

Insertion of (7) into (6) yields

$$\mu_i \frac{du(\tau, \mu_i)}{d\tau} = u(\tau, \mu_i) - \sum_{\substack{j=-N \\ j \neq 0}}^{N} w_j D(\tau, \mu_i, \mu_j) u(\tau, \mu_j)$$

$$- e^{-\alpha\tau} \sum_{l=0}^{K} X_l(\mu_i) \tau^l. \qquad (8)$$

We proceed by seeking a particular solution to (8) of the form

$$u_p(\tau, \mu_i) = e^{-\alpha\tau} \sum_{l=0}^{K} Y_l(\mu_i) \tau^l, \qquad (9)$$

where the $Y_l(\mu_i)$'s are coefficients to be determined. Substitution of (9) into (8) gives

$$\sum_{\substack{j=-N \\ j \neq 0}}^{N} \{\delta_{ij}(1 + \alpha\mu_i) - w_j D(\tau, \mu_i, \mu_j)\} Y_K(\mu_j) = X_K(\mu_i) \quad (10)$$

$$\sum_{\substack{j=-N \\ j \neq 0}}^{N} \{\delta_{ij}(1 + \alpha\mu_i) - w_j D(\tau, \mu_i, \mu_j)\} Y_l(\mu_j)$$

$$= \mu_i(l + 1) Y_{l+1}(\mu_i) + X_l(\mu_i),$$

$$l = K - 1, K - 2, ..., 0, \qquad (11)$$

which is a system of linear algebraic equations determining the $Y_l(\mu_i)$'s.

The general solution to Eq. (8) may then be written as

$$u(\tau, \mu_i) = \sum_{\substack{j=-N \\ j \neq 0}}^{N} C_j G_j(\mu_i) e^{k_j \tau} + e^{-\alpha\tau} \sum_{l=0}^{K} Y_l(\mu_i) \tau^l, \quad (12)$$

where the first sum on the right side is the solution of the homogeneous equation (see Ref. [10] for details).

2.1. Determination of the Coefficient α and $X_l(\mu)$

Different methods may be used to calculate α and the $X_l(\mu)$ coefficients in Eq. (7) for a given source. In the colocation approach the approximated source is required to equal the known source at certain points in the layer. Another approach is to enforce particle conservation by requiring

$$\int_{\tau_0}^{\tau_2} d\tau \, Q(\tau, \mu) = \int_{\tau_0}^{\tau_2} d\tau \, e^{-\alpha\tau} \sum_{l=0}^{K} X_l(\mu) \tau^l. \qquad (13)$$

Yet another approach related to the colocation method is to use fitting (e.g., a non-linear least-squares fit) to find the values of α and $X_l(\mu)$, yielding an approximated source that most closely resembles the actual source $Q(\tau, \mu)$.

Both the conservation and the fitting method require some iteration to find the coefficients and is therefore in general expected to be slower than the colocation procedure for which analytic expression may be derived for the α and $X_l(\mu)$ coefficients, regardless of the shape of the source. Since we are concerned about both speed and accuracy as well as ease of implementation, we choose to use the colocation procedure. From numerous applications of this procedure to solve neutral particle transport problems using a multi-group method, it has been verified that particle conservation is fulfilled [19].

If external forces, $F(r, p, t)$, or spherical geometry in Eq. (1), are important for the particular problem in question, then derivatives of the distribution function with respect to μ, the cosine of the polar angle, are required. The derivatives can be reliably calculated by evaluating the distribution function at two nearby angles, [15] and Ø. Lie-Svendsen (private communication, 1991). The present approach allows us to compute distribution functions at arbitrary angles and optical depths; see Appendix A.

3. NUMERICAL RESULTS

The accuracy of the approximation to the source term (7) will depend upon the choice of K and α. To examine the accuracy of different approximations we use thermal radiation in a scattering, absorbing, and emitting layered medium in local thermodynamic equilibrium, and a rapidly

varying beam pseudo-source in a scattering and absorbing medium as convenient examples.

The discrete ordinate method [10] was used to solve the radiative transfer equation for a highly absorbing medium $(\omega = 0.1)$ and a medium with little absorption $(\omega = 0.95)$. The phase function was taken to be the Heyney–Greenstein function [16] with asymmetry factor $g = 0.05$ (nearly isotropic scattering) for $\omega = 0.1$ and $g = 0.75$ (forward scattering) for $\omega = 0.95$. All computations were done in the 16-stream approximation $(2N = 16$, double Gaussian quadrature). Both optically thin and thick media were considered. The modifications to the theory given in [10], necessary to accomodate the quadratic and the exponential-linear approximations are provided in Section 2 and in the appendices.

For the Planck source the temperature was assumed to vary linearly across the layer and we compared the accuracy of fluxes and intensities incurred in different approximations. For the monodirectional beam pseudo-source we computed mean diffuse intensities for a single homogeneous layer. Depending on the angle of incidence of the beam this gives rise to an internal source that varies exponentially or less rapidly across the layer. The benchmark results used for checking the accuracy of the single layer results produced by subdividing this single layer into a large number of sublayers (50–100) to ensure convergence. The results of these comparisons are summarized below.

3.1. Thermal Radiation as an Internal Source

In previous works, [3, 11, 12, 13], the radiative transfer equation (5) has been solved with a linear-in-depth approximation of the Planck function, i.e., $\alpha = 0$ and $K = 1$ in (7). A linear approximation to the total source including the multiple scattering term in Eq. (5) has been considered in the neutron-transport context [14]. The errors incurred by approximating $B[T(\tau)]$ as a linear function in τ have been studied in Refs. [12, 13]. In the following we demonstrate the improvements obtained by invoking the quadratic $(K = 2$, $\alpha = 0$ in (15)) and, in particular, the exponential-linear-in-depth $(K = 1$, $\alpha \neq 0)$ approximations. The different approximations are compared for a homogeneous slab represented by a single layer with a specified temperature gradient. For simplicity we will assume that the temperature varies linearly across the layer in all examples to be considered below. This is a reasonable assumption for a medium in thermodynamic equilibrium [12]. Furthermore, it allows the Planck function to be evaluated at layer boundaries as well as arbitrary interior points as needed in the comparisons. A multilayer isothermal $(K = 0$, $\alpha = 0$ in (15)) calculation in which the temperature was allowed to vary from layer to layer, serves as a benchmark since this solution will converge to the correct result if a sufficiently large number of layers is utilized.
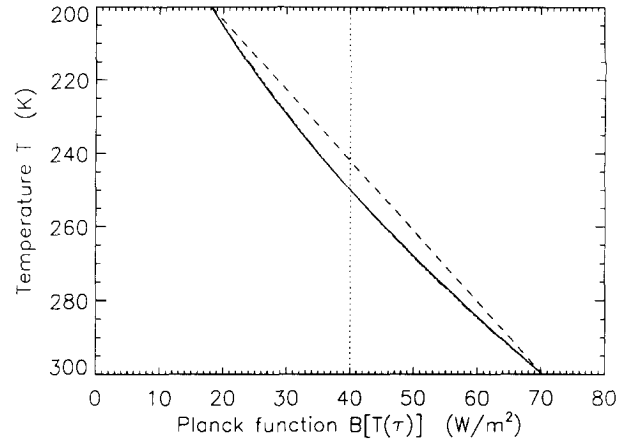

FIG. 1. The Planck function integrated over the spectral range 300–800 cm^{-1}, giving approximately a T^4 dependence (solid line) and the different approximations to it: isothermal (dotted line), and linear (dashed line). Both the quadratic and the exponential-linear approximations are indistinguishable from the Planck function itself.

Three different spectral regions giving rise to the Stefan–Boltzmann law, the Rayleigh–Jeans limit and the Wien limit are considered. In Fig. 1 we show the Planck function integrated over the entire spectrum and in Fig. 2 it is integrated over a small wavelength region in the Wien limit $(h\nu \gg kT)$. The different approximations to the source are also shown. In the Rayleigh–Jeans limit $(h\nu \ll kT)$, the source varies linearly with temperature and therefore with depth, Eq. (2).

For photon transport the source term for a medium in local thermodynamic equilibrium is [3]

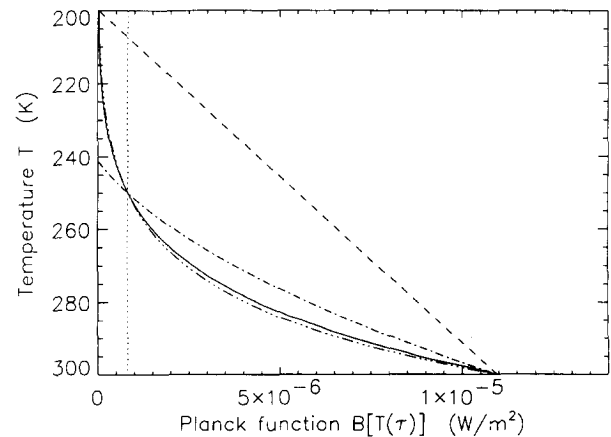$$Q(\tau, \mu, \phi) = Q(\tau) = [1 - \omega(\tau)] B[T(\tau)]. \qquad (14)$$

FIG. 2. The Planck function integrated over a narrow frequency range in the Wien limit (2702.99–2703.01 cm^{-1}). The solid line represents the Planck function, and the different approximations to it are the isothermal (dotted line), linear (dashed line), the quadratic (dash-dotted line), and the exponential-linear (dash-dashed line).

The Planck source term $B[T]$ is isotropic and may be approximated by

$$B[T(\tau)] = e^{-\alpha\tau} \sum_{l=0}^{K} b_l \tau^l, \qquad (15)$$

according to (7). We thus seek a particular solution of the form

$$u_p(\tau, \mu_i) = (1 - \omega(\tau)) e^{-\alpha\tau} \sum_{l=0}^{K} Y_l(\mu_i) \tau^l, \qquad (16)$$

implying that the $Y_l(\mu)$ coefficients are determined by solving Eqs. (10)–(11) with $X_l(\mu_i) = (1 - \omega) b_l$.

Integrating the Planck function over the entire spectral range we obtain the Stefan–Boltzmann law equation (4) which is applicable to gray media. We actually integrated over the wavenumber region 300–800 cm^{-1} which covers the major part of the Planck function for terrestrial temperatures. The quadratic and exponential-linear

approximations both agree very well with the Planck function for this case, as illustrated in Fig. 1. In Table I we compare fluxes in the Stefan–Boltzmann limit resulting from the isothermal, linear, quadratic, and exponential-linear approximations for a temperature difference $\Delta T = 100$ K across a single layer slab, with "correct" results obtained by subdividing the slab into 100 layers. As shown previously [12], the linear approximation is adequate for small temperature gradients, whereas for large temperature gradients, Table I, the quadratic and the exponential-linear approximation give the best results, as expected.

The energy deposition rate is proportional to the divergence of the net flux and plays an important role in a variety of problems. We calculate the net flux divergence by taking the difference between the mean intensity and the Planck function

$$\frac{1}{4\pi} \frac{dF(\tau)}{d\tau} = (1 - \omega(\tau))\{\overline{I(\tau)} - B[T(\tau)]\}. \qquad (17)$$

TABLE I

Sensitivity and Accuracy Comparison of Flux Computation for Thermal Emission in the Wavenumber Region 300–800 cm^{-1} with Various τ for $\omega = 0.1$ and $g = 0.05$ (in Parentheses for $\omega = 0.75$ and $g = 0.95$) in a Layer with Temperature 200 K at the Top and 300 K at the Bottom

(a) Flux divergence in layer (Net flux top - Net flux bottom) (W/m^2)

	Exponential-linear		Quadratic		Linear		Isothermal		
τ				1 layer					100 layers
0.1	−39.834	0.0%	−39.837	0.0%	−42.493	6.7%	−38.490	−3.4%	−39.839
	(−2.574)	0.0%	(−2.562)	0.1%	(−2.746)	6.6%	(−2.488)	−3.4%	(−2.575)
1.0	−195.320	0.0%	−195.335	0.0%	−207.497	6.2%	−187.947	−3.8%	−195.348
	(−24.133)	0.0%	(−24.134)	0.0%	(−25.747)	6.7%	(−23.321)	−3.4%	(−24.135)
10.0	−265.766	0.0%	−265.785	0.0%	−271.814	2.3%	−246.205	−7.4%	−265.788
	(−136.613)	0.0%	(−136.623)	0.0%	(−145.074)	6.2%	(−131.406)	−3.8%	(−136.632)
100.0	−271.111	0.1%	−271.114	0.1%	−271.817	0.3%	−246.207	−9.1%	−270.983
	(−172.104)	0.0%	(−172.114)	0.0%	(−175.041)	1.7%	(−158.550)	−7.9%	(−172.113)

(b) Upward flux at the top (W/m^2)

	Exponential-linear		Quadratic		Linear		Isothermal		
τ				1 layer					100 layers
0.1	19.274	0.0%	19.272	0.0%	20.600	6.9%	19.245	−0.1%	19.271
	(1.264)	0.0%	(1.262)	−0.2%	(1.351)	6.9%	(1.244)	−1.5%	(1.264)
1.0	80.298	0.2%	80.212	0.1%	86.294	7.7%	93.974	17.2%	80.164
	(11.322)	0.0%	(11.319)	0.0%	(12.125)	7.1%	(11.661)	3.0%	(11.317)
10.0	64.001	0.4%	63.817	0.1%	66.832	4.9%	123.103	93.2%	63.725
	(53.122)	0.2%	(53.045)	0.1%	(57.271)	8.1%	(65.703)	24.0%	(53.001)
100.0	56.444	−0.2%	56.415	−0.2%	56.767	0.4%	123.104	117.7%	56.541
	(39.569)	0.4%	(39.470)	0.1%	(40.933)	3.8%	(79.275)	101.1%	(39.423)

Figure 3 shows the relative error in the right-hand side of (17) that results from the isothermal, linear, quadratic, and exponential-linear approximations to the Planck-function in the Stefan-Boltzmann limit. Again a 100-layer calculation served as the benchmark. Clearly the quadratic and the exponential-linear approximations work very well, whereas the errors for the isothermal and linear approximations are substantial.

The exponential-linear behavior of the Planck function in the Wien limit, cf. Eq. (3) is fitted nicely by the exponential-linear approximation, whereas the isothermal, linear, and quadratic approximations all fail (see Fig. 2). In Table II we give the upward $(\mu = 1)$ and downward $(\mu = -1)$ intensities for the Planck function integrated over the wavenumber interval 2702.99–2703.01 cm^{-1} $(\approx 3.7 \mu m$, the bandpass center of one of the channels on the AVHRR (advanced very high resolution radiometer) instrument
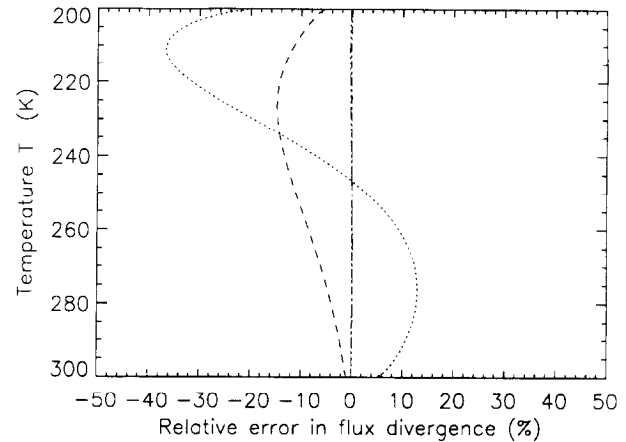

Fig. 3. The relative errors in the flux divergence for the Stefan-Boltzmann case for a temperature gradient of $\Delta = 100$ K across the layer for $g = 0.75$ and $\omega = 0.95$.

TABLE II

Upward and Downward Intensities for the Wavenumber Region 2702.99–2703.01 cm^{-1} (Wien limit) for a Layer with Temperature 200 K at the Top and 300 K at the Bottom.

(a) Upward intensity $(\mu = 1)$ at top $(10^{-7} W/m^2 ster)$

τ	Exponential-linear		Quadratic		Linear		Isothermal		50 layers
				1 layer					
0.1	1.802	−4.1%	1.990	6.0%	4.703	150.0%	0.714	−62.0%	1.878
	(0.111)	−4.0%	(0.121)	5.2%	(2.844)	2400.0%	(0.042)	−63.1%	(0.115)
1.0	9.266	−3.8%	9.410	−2.3%	28.04	200.0%	4.971	−48.4%	9.631
	(1.264)	−4.1%	(1.402)	6.4%	(3.330)	150.0%	(0.502)	−61.9%	(1.318)
10.0	0.817	13.1%	−3.820	−630.0%	11.27	1460.0%	8.081	100.0%	0.723
	(6.131)	−3.3%	(5.292)	−16.6%	(23.39)	270.0%	(4.699)	−25.9%	(6.343)
100.0	0.194	2.3%	−0.581	−400.0%	28.04	14700.0%	8.082	4160.0%	0.190
	(0.282)	18.5%	(−2.264)	−1050.0%	(4.631)	1850.0%	(5.933)	2400.0%	(0.238)

(b) Downward intensity $(\mu = -1)$ at bottom $(10^{-6} W/m^2 ster)$

τ	Exponential-linear		Quadratic		Linear		Isothermal		50 layers
				1 layer					
0.1	0.192	−1.4%	0.215	7.4%	0.486	143.0%	0.071	−64.3%	0.200
	(0.011)	−4.1%	(0.013)	13.3%	(0.028)	146.8%	(0.004)	−63.1%	(0.012)
1.0	1.707	−4.2%	1.987	11.6%	3.850	116.2%	0.497	−72.1%	1.781
	(0.131)	−4.1%	(0.146)	7.0%	(0.339)	148.4%	(0.050)	−63.2%	(0.136)
10.0	7.151	−3.2%	8.182	10.8%	9.691	31.2%	0.808	−89.1%	7.388
	(1.779)	−4.5%	(2.141)	15.0%	(3.951)	110.0%	(0.470)	−74.8%	(1.862)
100.0	10.28	0.1%	10.50	2.2%	3.850	−62.5%	0.808	−92.1%	10.27
	(6.166)	−2.6%	(6.790)	7.3%	(7.480)	18.2%	(0.593)	−90.6%	(6.329)

Note. Single scattering albedo and asymmetry factor as in Table I.

flown on the NOAA TIROS satellite), as calculated by the different approximations. As expected from Fig. 2, only the exponential-linear approximation comes close to the "correct" multilayer result. The quadratic approximation even gives negative (unphysical) upward intensities for a highly absorbing atmosphere, see Table II. This is readily understood by examining Fig. 2.

Finally, in the Rayleigh–Jeans limit, cf. Eq. (2), the Planck function exhibits a linear in $T(\tau)$ dependence. All approximations work well in this limit, except the isothermal one which may be off by as much as 20% for optical thicknesses greater than 10.

3.2. The Monodirectional Beam Pseudo-Source

To demonstrate how the exponential-linear approximation works for anisotropic sources we consider the example of a direct beam incident on a scattering and absorbing medium. To handle a monodirectional incident beam it is common to use the diffuse-direct radiation splitting procedure [3]. In slab geometry this leaves us with an equation for the diffuse radiation of the form identical to Eq. (6) with

$$Q(\tau, \mu) = \frac{\omega(\tau)}{4\pi} P(\mu, \mu_0) I_0 e^{-\tau/\mu_0}, \qquad (18)$$

where I_0 is the intensity of the incoming beam, $P(\mu, \mu_0)$ is the azimuthally averaged phase function, and μ_0 is the cosine of the angle of incidence. This source term has an exact exponential behavior and may be solved analytically [10]. (We have verified that our exponential-linear approximation yields results that are identical to the analytic solution as required when Eq. (18) is used.) In spherical geometry the argument of the exponential in Eq. (18) is replaced by a more slowly varying function, generically referred to as the Chapman function $ch(\tau, \mu_0)$ [15],

$$Q(\tau, \mu) = \frac{\omega(\tau)}{4\pi} P(\mu, \mu_0) I_0 e^{-ch(\tau, \mu_0)}. \qquad (19)$$

As long as $\mu_0 > 0$, solution of the multiple scattering problem in slab geometry yields sufficient accuracy for many applications, provided the primary scattering driving term, Eq. (19), is computed correctly using spherical geometry [15].

Previous attempts [15] to approximate the pseudo-source term given by Eq. (19) with a sum of exponential functions (one for each layer in a multi-layered medium) did not yield satisfactory results. A purely exponential approximation reproduces the actual source at one point in the layer and will be very sensitive to the chosen point. A linear-in-optical depth approximation reproduces the source at layer boundaries and yields adequate results if the scattering depth of any layer is not too large [15]. For layers with a large scattering depth, a linear function is a rather poor approximation to a very rapidly varying function. The exponential-linear approximation resembles the actual source term much better as illustrated in Figs. 4 and 5.

Figures 4 and 5 also give the diffuse radiation as governed by Eqs. (6) and (19) for beam angles of 70° (Fig. 4), and 85° (Fig. 5). At 70° the curvature effects are small and the beam pseudo-source has essentially an exponential behavior which is nicely fitted with the exponential-linear approximation. The linear approximation gives unacceptably large errors, even for a medium with moderate scattering depth, $\tau = 1.0$. For 85°, curvature effects come into play and the beam pseudo-source falls off more slowly with optical depth than in a plane parallel medium. In this case the exponential-linear approximation overestimates the diffuse radiation by about 15%. But this is still much better than the linear approximation which overestimates the diffuse radiation by several hundred percent. We also investigated similar examples for a scattering depth of $\tau = 10.0$. The exponential-linear approximation behaves well for angles where curvature effects are negligible, but was off by 50–100% for large angles of incidence. The linear approximation overestimated the diffuse radiation by several orders of magnitude for large scattering depths.
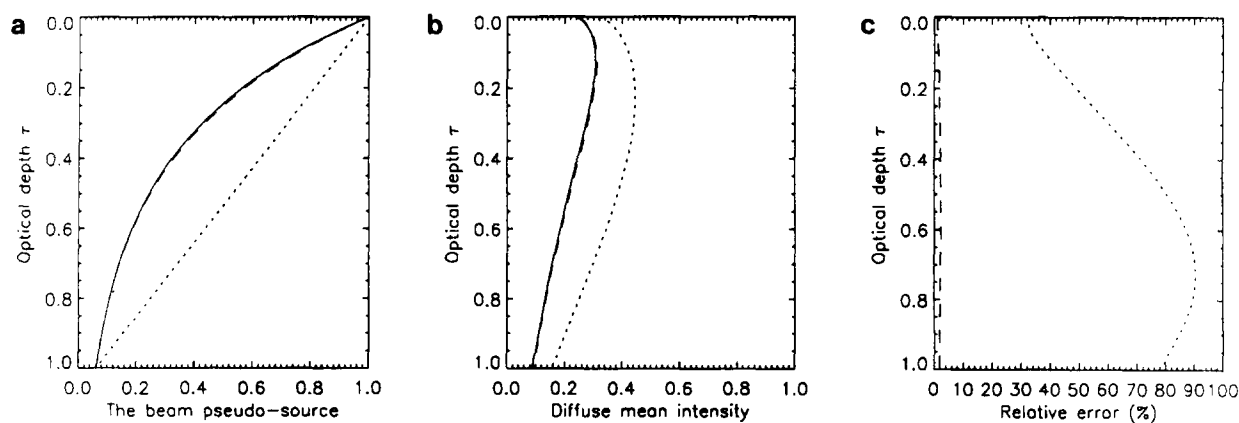
Fig. 4. (a) The beam pseudo-source for $\theta = \arccos \mu_0 = 70°$ (solid line) and the linear (dashed line) and the exponential-linear (dash-dashed line) approximations to it. (b) The mean diffuse intensity, arbitrary units. (c) The relative error for the different approximations.
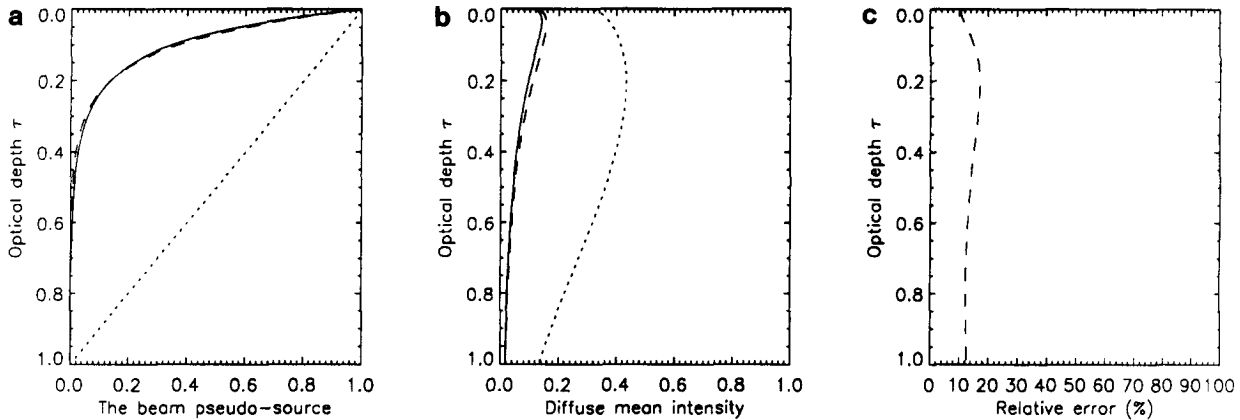
Fig. 5. Same as Fig. 4, but for $\theta = \arccos \mu_0 = 85°$. Note that in (c) the error for the linear approximation is so large that it is off the graph.

3.3. Summary of Results

For thermal radiation we find that in the case of the Stefan–Boltzmann law the quadratic and the exponential-linear approximations give the smallest errors in boundary fluxes and intensities as well as energy deposition rates, for both small and large temperature gradients. The improvement from an isothermal to a linear approximation is already substantial in this case for as small a temperature difference as 10 K. There is little to gain with the quadratic or the exponential-linear approximation for small temperature gradients. However, for large temperature gradients the quadratic and the exponential-linear approximations both give good results, whereas the linear approximation tends to overestimate the boundary fluxes and intensities and underestimate energy deposition rates. The Rayleigh–Jeans limit is nicely approximated by all but the isothermal method, whereas only the exponential-linear approximation works well in the Wien limit.

As expected, the monodirectional beam pseudo-source is nicely fitted by the exponential-linear approximation for beam angles where curvature effects are small or can be neglected. When curvature effects become large the exponential-linear approximation gives increasingly larger errors with increasing scattering depths. The errors may be removed by increasing the number of layers. The linear approximation gives unacceptably large errors for any angle and even for moderate scattering depths.

All the computations were done in single precision on a 32-bit computer (VAX 8800). The increase in run time of the quadratic and the exponential-linear over the linear approximation is negligible. In fact, the run time will in general decrease substantially as fewer layers will be necessary to obtain the same level of accuracy.

4. DISCUSSION

In many circumstances the internal source will be known only at the computational mesh points chosen to obtain a numerical solution to Eq. (5). Thus, in most practical applications we are likely to know the term $Q(\tau_k, \mu_i)$ in Eq. (5) only for a set of discrete values τ_k with $k = 1, 2, ..., L$ and μ_i with $i = \pm 1, \pm 2, ..., \pm N$. The functional behavior of $Q(\tau, \mu)$ between any of these grid points may not in general be available. Focusing on how to obtain an optimal approximation of the spatial variation of the source term Q, we see that the linear approximation may be the best we can do if nothing is known about the behavior of Q in the interval $\tau_{k-1} < \tau < \tau_k$, $k = 1, 2, ..., L$.

The computational examples given in Section 3 illustrate however, that if we know the source term at one additional point (say mid-point) in each layer $\tau_{k-1} < \tau < \tau_k$, then the quadratic and exponential-linear approximations offer distinct advantages. If a general-purpose particle transport code such as that described in [10] is used to provide solutions, there will be no problem in generating the internal source term at depths other than the computational mesh points (as needed in the exponential-linear approximation), because that code allows for the distribution function to be computed at arbitrary depths.

To investigate the different approximations, we have used the Planck function in our numerical demonstrations mainly because its analytical form allows us to compute the source term at arbitrary interior points for a given temperature variation. Applications of the Planck function in different spectral ranges also allows us to explore the performance of the various approximations for sources that vary both rapidly (Stefan–Boltzmann law and Wien limit) and slowly (Rayleigh–Jeans limit) with depth. Thus, while the Planck function was chosen merely as a convenient analytic tool for testing the accuracy of the various approximations and the beam pseudo-source was chosen to demonstrate that the exponential-linear approximation works well also for anisotropic sources, we expect the numerical examples given in this paper to provide a good indication of the performance of these approximations in general, at least for sources that vary monotonically in each layer of the slab.

For particle transport driven by boundary sources, the internal source term may be due to internal production of secondary or energy degraded particles. In this case the internal source is expected to have a rapid, near-exponential variation with depth, and we anticipate the exponential-linear approximation to work well. Furthermore, large (essentially semi-infinite) scattering depths are a common occurrence in many particle transport problems. Under such circumstances the exponential-linear approximation becomes extremely valuable. In fact, a linear approximation may become impractical due to the large mesh size required to obtain reasonable accuracy.

The exponential-linear approximation is routinely used by the authors in a variety of radiative transfer calculations including twilight conditions and has proven to be more accurate than the linear approximation [15]. The method is also used in neutral particle transport calculations [19] and has been found to be both more accurate and computationally more efficient than the linear approximation. This is a matter of some practical importance because iterations are frequently used to solve particle transport problems when "upscattering" occurs, i.e., test particle thermalization problems and problems where forces are present [5, 19]. Such iterations typically require repeated solutions of the transport equation, implying that an efficient solution is indeed very desirable [19]. Finally, improved energy conservation has been achieved by using the exponential-linear instead of the linear approximation in electron transport calculations (D. Lummerzheim 1991, private communication).

5. CONCLUSION

The transport equation for monoenergetic particles has been solved for a general anisotropic, spatially varying source term in slab geometry. Numerical examples pertinent for thermal radiation in a scattering, absorbing, and emitting medium as well as for a monodirectional beam pseudo-source in a scattering and absorbing medium, are used to illustrate the errors incurred by invoking different approximations to the source term in the transport equation. A new exponential-linear in-depth approximation to the internal source is found to provide both high accuracy and computational efficiency for a variety of circumstances likely to be encountered in practice, including steep gradients in the source and large scattering depths for which a linear approximation becomes impractical due to the large spatial mesh size required to obtain adequate accuracy.

Specific examples including internal sources that vary slowly as well as rapidly with depth indicate that this approximation will, in general, provide adequate accuracy for most practical applications. In particular, the exponential-linear approximation yields very accurate intensities,

fluxes, and energy deposition rates in the presence of large gradients in the source term which may be imposed by the physics of the problem or else by our desire to use large increments in spatial step size to save computer time.

The numerical code is stable, computationally efficient, and lends itself readily to the solution of a variety of physical problems including neutral and charged particle transport as well as linearized gas dynamics. A computer code for solving the thermal radiation problem (with the Planck function as an internal source) using the exponential-linear approximation is available to interested users [10, 17].

APPENDIX A: ANGULAR DISTRIBUTIONS AND THE b_l COEFFICIENTS

To calculate the intensities given in Tables I and II and Figs. 3–5 the theory outlined in [10] had to be modified. The changes necessary for the quadratic and the exponential-linear approximations are given below.

A.1. The Polynomial In-depth Approximation

Approximating the source by a polynomial, $\alpha = 0$ in Eq. (15), gives K linear equations to solve for the b_l coefficients. Analytic solutions to these equations are preferred as we then can easily calculate intensities at any depth and angle, using the interpolating scheme outlined in [10]. The extensions necessary to the theory outlined in [10] are given for the quadratic-in-depth approximation below.

A.1.1. *The b_l coefficients for $K = 2$, $\alpha = 0$.* To evaluate the b_l coefficients in (15), three equations are needed for the three coefficients b_0, b_1, and b_2 for each layer. Knowing the temperature at layer interfaces ($T(\tau_0)$ and $T(\tau_2)$) we may write

$$B_0 = B[T(\tau_0)] = b_0 + b_1\tau_0 + b_2\tau_0^2 \qquad (20)$$

$$B_1 = B[T(\tau_1)] = b_0 + b_1\tau_1 + b_2\tau_1^2 \qquad (21)$$

$$B_2 = B[T(\tau_2)] = b_0 + b_1\tau_2 + b_2\tau_2^2, \qquad (22)$$

where τ_0, τ_1, and τ_2 are the optical depths at the top, center, and bottom of the layer, respectively. Assuming that $T(\tau_1) = (T(\tau_0) + T(\tau_2))/2$ and $\tau_1 = (\tau_0 + \tau_2)/2$, we readily solve (20)–(22) to yield

$$b_2 = \frac{\frac{1}{2}B_2 - B_1 + \frac{1}{2}B_0}{\frac{1}{4}(\tau_2 - \tau_0)^2} \qquad (23)$$

$$b_1 = \frac{B_2 - B_0}{\tau_2 - \tau_0} - b_2(\tau_2 + \tau_0) \qquad (24)$$

$$b_0 = B_0 - b_1\tau_0 - b_2\tau_0^2. \qquad (25)$$

A.1.2. *Angular distributions.* The radiative transfer equation is solved for $K = 2$ following [10]. By using the interpolation technique discussed in [18] the intensities may be calculated at any angle and depth. For the quadratic approximation the upward intensity is given by (see Eq. (25) in [10])

$$u_p(\tau, +\mu) = u(\tau_L, +\mu) \exp[-(\tau_L - \tau)/\mu]$$
$$+ \frac{G_{0n}(+\mu)}{1 + \mu/\mu_0} E_{0n}(\tau, +\mu)$$
$$+ \sum_{n=p}^{L} \left\{ \sum_{j=1}^{N} \left[\tilde{C}_{-jn} \frac{G_{-jn}(+\mu)}{1 - k_{jn}\mu} E_{-jn}(\tau, +\mu) \right. \right.$$
$$\left. + \tilde{C}_{+jn} \frac{G_{+jn}(+\mu)}{1 + k_{jn}\mu} E_{+jn}(\tau, +\mu) \right]$$
$$+ \delta_{m0}[V_{0n}(+\mu) F_{0n}(\tau, +\mu)$$
$$\left. + V_{1n}(+\mu) F_{1n}(\tau, +\mu) + V_{2n} F_{2n}(\tau, +\mu)] \right\},$$
$$\tag{26}$$

where

$$E_{-jn}(\tau, +\mu) = \exp[-(k_{jn} \Delta\tau_n - \delta\tau/\mu]$$
$$- \exp[-(\tau_n - \tau)/\mu] \tag{27}$$

$$F_{0n}(\tau, +\mu) = \exp(-\delta\tau/\mu) - \exp[-(\tau_n - \tau)/\mu] \tag{28}$$

$$F_{1n}(\tau, +\mu) = (\tau_{n-1} + \mu) \exp(-\delta\tau/\mu)$$
$$- (\tau_n + \mu) \exp[-(\tau_n - \tau)/\mu] \tag{29}$$

$$F_{2n}(\tau, +\mu) = (\tau_{n-1}^2 + 2\mu\tau_{n-1} + 2\mu^2) \exp(-\delta\tau/\mu)$$
$$- (\tau_n^2 + 2\mu\tau_n + 2\mu^2) \exp[-(\tau_n - \tau)/\mu] \tag{30}$$

with $\delta\tau = \tau_{n-1} - \tau$ for $n > p$ and $\delta\tau = 0$ for $n = p$, $\Delta\tau_n = \tau_n - \tau_{n-1}$ for $n > p$ and $\Delta\tau_p = \tau_p - \tau$ for $n = p$,

$$E_{+jn}(\tau, +\mu) = \exp[-(\tau_{n-1} - \tau)/\mu]$$
$$- \exp\{-[k_{jn}(\tau_n - \tau_{n-1}) - (\tau - \tau_n)/\mu]\} \tag{31}$$

for $n > p$ and

$$E_{+jp}(\tau, +\mu) = \exp[-k_{jp}(\tau - \tau_{p-1})]$$
$$- \exp\{-[k_{jp}(\tau_p - \tau_{p-1}) + (\tau_p - \tau)/\mu]\}. \tag{32}$$

For the downward intensity (Eq. (26) in [10]), we find

$$u_p(\tau, -\mu) = u(0, -\mu) \exp[-\tau/\mu] + \frac{G_{0n}(-\mu)}{1 - \mu/\mu_0} E_{0n}(\tau, -\mu)$$
$$+ \sum_{n=1}^{p} \left\{ \sum_{j=1}^{N} \left[\tilde{C}_{-jn} \frac{G_{-jn}(-\mu)}{1 + k_{jn}\mu} E_{-jn}(\tau, -\mu) \right. \right.$$
$$\left. + \tilde{C}_{+jn} \frac{G_{+jn}(-\mu)}{1 - k_{jn}\mu} E_{+jn}(\tau, -\mu) \right]$$
$$+ \delta_{m0}[V_{0n}(-\mu) F_{0n}(\tau, -\mu)$$
$$\left. + V_{1n}(-\mu) F_{1n}(\tau, -\mu) + V_{2n} F_{2n}(\tau, -\mu)] \right\},$$
$$\tag{33}$$

where

$$E_{+jn}(\tau, -\mu) = \exp[-(k_{jn} \Delta\tau_n + \delta\tau/\mu]$$
$$- \exp[-(\tau - \tau_{n-1})/\mu] \tag{34}$$

$$F_{0n}(\tau, -\mu) = \exp(-\delta\tau/\mu) - \exp[-(\tau - \tau_{n-1})/\mu] \tag{35}$$

$$F_{1n}(\tau, -\mu) = (\tau_n - \mu) \exp(-\delta\tau/\mu)$$
$$- (\tau_{n-1} - \mu) \exp[-(\tau - \tau_{n-1})/\mu] \tag{36}$$

$$F_{2n}(\tau, -\mu) = (\tau_n^2 - 2\mu\tau_n + 2\mu^2) \exp(-\delta\tau/\mu)$$
$$- (\tau_{n-1}^2 - 2\mu\tau_{n-1} + 2\mu^2)$$
$$\times \exp[-(\tau - \tau_{n-1})/\mu] \tag{37}$$

with $\delta\tau = \tau - \tau_n$ for $n < p$ and $\delta\tau = 0$ for $n = p$, $\Delta\tau_n = \tau_n - \tau_{n-1}$ for $n < p$ and $\Delta\tau_p = \tau - \tau_{p-1}$ for $n = p$,

$$E_{-jn}(\tau, -\mu) = \exp[-(\tau - \tau_n)/\mu]$$
$$- \exp\{-[k_{jn}(\tau_n - \tau_{n-1})$$
$$+ (\tau - \tau_{n-1})/\mu]\} \tag{38}$$

for $n < p$ and

$$E_{-jp}(\tau, -\mu) = \exp[-k_{jp}(\tau_p - \tau)]$$
$$- \exp\{-[k_{jp}(\tau_p - \tau_{p-1}) + (\tau - \tau_{p-1})/\mu]\} \tag{39}$$

$$V_l(\mu) = \sum_{\substack{i=-N \\ i \neq 0}}^{N} w_i D(\mu, \mu_i) Y_l(\mu_i) + (1 - \omega) b_l,$$
$$l = 2, 1, 0. \tag{40}$$

A.2. The Exponential-Polynomial Approximation

For $\alpha \neq 0$, Eq. (7) is a set of non-linear equations determining α and the $X_l(\mu)$ coefficients. This set of equations may not be readily solved for any value of K by analytical methods. However, for $K \leq 3$ analytic solutions exist. For $K = 1$ we have the exponential-linear approximation.

A.3. The b_i Coefficients for $K = 1$, $\alpha \neq 0$

Knowing the internal source Q_i for each layer at the top, center, and bottom we obtain three equations to solve for the three unknown coefficients,

$$Q_0(\mu) = e^{-\alpha\tau_0}(X_0(\mu) + X_1(\mu)\,\tau_0) \tag{41}$$

$$Q_1(\mu) = e^{-\alpha\tau_1}(X_0(\mu) + X_1(\mu)\,\tau_1) \tag{42}$$

$$Q_2(\mu) = e^{-\alpha\tau_2}(X_0(\mu) + X_1(\mu)\,\tau_2). \tag{43}$$

For each layer the temperature is known at the top and bottom of the layer ($T(\tau_0)$ and $T(\tau_2)$). Assuming $T(\tau_1) = (T(\tau_0) + T(\tau_2))/2$ and $\tau_1 = (\tau_0 + \tau_2)/2$ we can calculate the Planck function at the top, center, and bottom of the layer. Solving (41)–(43) with $Q_i = B[T(\tau_i)] = B_i$ the coefficients in Eq. (15) are

$$\alpha = \frac{2}{\tau_2 - \tau_0}\ln\left\{\frac{B_1}{B_2} \pm \sqrt{(B_1/B_2)^2 - B_0/B_2}\right\} \tag{44}$$

$$b_1 = \frac{B_2 e^{\alpha\tau_2} - B_0 e^{\alpha\tau_0}}{\tau_2 - \tau_0} \tag{45}$$

$$b_0 = B_0 e^{\alpha\tau_0} - b_1\tau_0. \tag{46}$$

We force the α coefficient to be angle independent by solving Eqs. (41)–(43) for one specific μ_i. All the angle dependence is in the $X_i(\mu)$ coefficients. Assuming $\tau_1 = (\tau_0 + \tau_2)/2$ the equations for α and $X_i(\mu_i)$ become

$$\alpha = \frac{2}{\tau_2 - \tau_0}\ln\left\{\frac{Q_1(\mu_1)}{Q_2(\mu_1)}\right.$$
$$\left. \pm \sqrt{(Q_1(\mu_1)/Q_2(\mu_1))^2 - Q_0(\mu_1)/Q_2(\mu_1)}\right\} \tag{47}$$

$$X_1(\mu_i) = \frac{Q_2(\mu_i)\,e^{\alpha\tau_2} - Q_0(\mu_i)\,e^{\alpha\tau_0}}{\tau_2 - \tau_0} \tag{48}$$

$$X_0(\mu_i) = Q_0(\mu_i)\,e^{\alpha\tau_0} - X_1(\mu_i)\,\tau_0,$$
$$i = \pm 1, \pm 2, ..., \pm N. \tag{49}$$

To calculate α from Eq. (47) we must have $Q_1^2 - Q_0 Q_2 \geq 0$. It is shown in Appendix B that this is always the case when the internal source is the Planck function. For sources where $Q_2 > Q_1 > Q_0$, we use the $(+)$ solution for α and the $(-)$ solution when $Q_2 < Q_1 < Q_0$. For source functions that decrease very rapidly with scattering depth, Q_2 (the source at the bottom) may be equal to zero. In this case we obtain for the coefficients

$$\alpha = \frac{2}{\tau_2 - \tau_0}\ln\left\{\frac{Q_0(\mu_1)}{Q_1(\mu_1)}\right\} \tag{50}$$

$$X_1(\mu_i) = 0 \tag{51}$$

$$X_0(\mu_i) = Q_0(\mu_i)\,e^{\alpha\tau_0}. \tag{52}$$

If both $Q_2 = 0$ and $Q_1 = 0$, we set $X_1(\mu_i) = 0$, $X_0(\mu_i) =$

$Q_0(\mu_i)$, and $\alpha = \max/\tau_2$ where $\max$ is the largest number available on the computer.

When the absolute value of α becomes large, numerical overflow problems may occur in either Eqs. (48)–(49) or Eq. (7). The value of α is most likely to blow up because $\tau_2 - \tau_0$ becomes small. For optically thin layers, however, the linear approximation gives adequate results. Thus when the absolute value of α is large enough to cause overflow, we set $\alpha = 0$ and use the linear approximation.

For completeness we note that values of α equal to any of the eigenvalues require special consideration because the particular solution due to an internal source proportional to $\exp(-k\tau)$ is proportional to $\tau\exp(-k\tau)$. Numerically this case may, however, be efficiently handled by so-called "dithering," by which any value of α deviating from an eigenvalue by less than a prescribed amount is changed to make the deviation slightly bigger. The actual amount of dithering depends on machine architecture. We have found that keeping α 1% away from an eigenvalue yields satisfactory results on a 32-bit machine in single precision.

A.3.1. Angular distribution.

For the exponential-linear approximation, the different factors in (26) and (33) become

$$F_{0n}(\tau, +\mu) = \frac{1}{\alpha_n\mu + 1}\{\exp(-C_1)\exp(-\delta\tau/\mu)$$
$$- \exp(-\alpha_n\tau_n)\exp[-(\tau_n - \tau)/\mu]\} \tag{53}$$

$$F_{1n}(\tau, +\mu) = \frac{1}{\alpha_n\mu + 1}\left\{\left(\tau_{n-1} + \frac{\mu}{\alpha_n\mu + 1}\right)\right.$$
$$\times \exp(-C_1)\exp(-\delta\tau/\mu)$$
$$- \left(\tau_n + \frac{\mu}{\alpha_n\mu + 1}\right)$$
$$\left. \times \exp(-\alpha_n\tau_n)\exp[-(\tau_n - \tau)/\mu]\right\} \tag{54}$$

$$F_{2n}(\tau, +\mu) = 0 \tag{55}$$

with $C_1 = \alpha_n\tau_{n-1}$ for $n > p$ and $C_1 = \alpha_n\tau$ for $n = p$,

$$F_{0n}(\tau, -\mu) = \frac{1}{\alpha_n\mu - 1}\{\exp(-C_1)\exp[-(\tau - \tau_{n-1})/\mu]$$
$$- \exp(-C_2)\exp(-\delta\tau/\mu)\} \tag{56}$$

$$F_{1n}(\tau, -\mu) = \frac{1}{\alpha_n\mu - 1}\left\{\left(\tau_{n-1} + \frac{\mu}{\alpha_n\mu - 1}\right)\right.$$
$$\times \exp(-C_1)\exp[-(\tau - \tau_{n-1})/\mu]$$
$$\left. - \left(\tau_n + \frac{\mu}{\alpha_n\mu - 1}\right)\exp(-C_2)\exp(-\delta\tau/\mu)\right\}$$
$$\tag{57}$$

$$F_{2n}(\tau, -\mu) = 0 \tag{58}$$

with $C_1 = \alpha_n\tau_{n-1}$ for $n < p$ and $C_1 = 0$ for $n = p$ and $C_2 = \alpha_n\tau_n$ for $n < p$ and $C_2 = \alpha_n\tau$ for $n = p$.

APPENDIX B: THE EXISTENCE OF THE α COEFFICIENT FOR THERMAL RADIATION

The α coefficient will always exist if $B_1^2/B_2^2 - B_0/B_2 > 0$ or, since $B_2 > 0$ for the Planck function, $B_1^2 - B_0 B_2 > 0$. The Planck function integrated over an arbitrary frequency interval is given by

$$B_i = B(T_i) = \int_{v_1}^{v_2} \frac{2hv^3}{c^2} \frac{dv}{\exp(hv/kT_i) - 1}. \tag{59}$$

Using Eq. (59) we find that the inequelity $B_1^2 - B_0 B_2 > 0$ is fulfilled if

$$\left(\exp\left(\frac{hv}{kT_2}\right) - 1\right)\left(\exp\left(\frac{hv'}{kT_0}\right) - 1\right)$$
$$- \left(\exp\left(\frac{hv}{kT_1}\right) - 1\right)\left(\exp\left(\frac{hv'}{kT_1}\right) - 1\right) > 0, \tag{60}$$

since $e^{hv/kT} > 1$ for $v > 0$ and $T > 0$. Using the relation

$$e^x - 1 = \sum_{n=1}^{\infty} \frac{x^n}{n!}, \tag{61}$$

the left-hand side of Eq. (60) may be written as

$$\sum_{n=1}^{\infty} \frac{(hv/kT_2)^n}{n!} \sum_{m=1}^{\infty} \frac{(hv'/kT_0)^m}{m!}$$
$$- \sum_{n=1}^{\infty} \frac{(hv/kT_1)^n}{n!} \sum_{m=1}^{\infty} \frac{(hv'/kT_1)^m}{m!}$$
$$= \sum_{n=1}^{\infty} \sum_{m=1}^{\infty} \frac{h^{n+m}}{k}$$
$$\times \left\{\frac{v^n v'^m}{n! \, m!} \left(\frac{1}{T_2^n T_0^m} - \frac{1}{T_1^{n+m}}\right)\right\}. \tag{62}$$

In general, $T_2^n T_0^m$ is not less than $T_1^{n+m} = ((T_0 + T_2)/2)^{n+m}$. However, for terms with $n = m$,

$$\frac{1}{T_2^n} \frac{1}{T_0^n} - \frac{1}{T_1^{2n}} = \left(\frac{1}{T_2 T_0}\right)^n - \left(\frac{1}{T_1^2}\right)^n > 0, \tag{63}$$

since $T_1^2 = ((T_0 + T_2)/2)^2 = \frac{1}{4}(T_0 - T_2)^2 + T_0 T_2 > T_0 T_2$. For terms with $n > m$, we set $n = m + l$, $l > 0$, and obtain

$$\frac{1}{T_2^n} \frac{1}{T_0^m} - \frac{1}{T_1^{n+m}} = T_2^l \left(\frac{1}{T_2 T_0}\right)^m - T_1^l \left(\frac{1}{T_1^2}\right)^m \tag{64}$$

and, for terms with $n < m$, we set $n = m - l$, $l > 0$ to obtain

$$\frac{1}{T_2^n} \frac{1}{T_0^m} - \frac{1}{T_1^{n+m}} = T_2^l \left(\frac{1}{T_2 T_0}\right)^m - T_1^l \left(\frac{1}{T_1^2}\right)^m. \tag{65}$$

For $T_2 > T_1 > T_0 \gg 1$ we may ignore the terms given by (64) while (65) is always positive. For $T_2 < T_1 \ll 1$ we may ignore (65) and (64) is then always positive. A similar argument may be used for the case $T_0 > T_1 > T_2 \gg 1$ and $T_0 < T_1 \ll 1$, by rewriting Eqs. (64)–(65) (set $m = n - l$ in (64) and $m = n + l$ in (65)).

For typical terrestrial and stellar temperatures ($T_i > 100$ K) we thus have that Eq. (62) is always positive, implying that the condition $B_1^2 - B_0 B_2 > 0$ is always fulfilled for the Planck function integrated over an arbitrary frequency interval. Thus the α coefficient exists for most realistic applications.

REFERENCES

1. K. M. Case and P. F. Zweifel, *Linear Transport Theory* (Addison-Wesley, Reading, MA, 1967).
2. C. Cerignani, *Theory and Application of the Boltzmann Equation* (Elsevier, New York, 1975).
3. S. Chandrasekhar, *Radiative Transfer* (Dover, New York, 1960).
4. B. Davison, *Neutron Transport Theory* (Oxford Univ. Press, London, 1957).
5. J. J. Duderstadt and W. R. Martin, *Transport Theory* (Wiley, New York, 1979).
6. M. R. Hoare, *Adv. Chem. Phys.* **20**, 135 (1971).
7. J. H. Ferziger and H. G. Kaper, *Mathematical Theory of Transport Processes in Gases* (North Holland, Amsterdam, 1972).
8. M. M. R. Williams, *The Slowing Down and Thermalization of Neutrons* (North Holland, Amsterdam, 1966).
9. K. Stamnes, *Rev. Geophys.* **24**, 299 (1986).
10. K. Stamnes, S.-C. Tsay, W. Wiscombe, and K. Jayaweera, *Appl. Opt.* **27**, 2502 (1988).
11. K. Stamnes and R. A. Swanson, *J. Atmos. Sci.* **38**, 387 (1981).
12. S.-C. Tsay, K. Stamnes, and K. Jayaweera, *J. Quant. Spectrosc. Radiat. Transfer* **43**, 133 (1990).
13. W. J. Wiscombe, *J. Quant. Spectrosc. Radiat. Transfer* **16**, 477 (1976).
14. R. E. Alcouffe, E. W. Larsen, W. F. Miller, Jr., and B. R. Wlenke, *Nucl. Sci. Eng.* **71**, 111 (1979).
15. A. Dahlback and K. Stamnes, *Planet. Space Sci.* **39**, 671 (1991).
16. L. C. Heyney and J. L. Greenstein, *Astrophys. J.* **93**, 70 (1941).
17. K. Stamnes, S.-C. Tsay, and W. Wiscombe, *NASA Tech. Rep.*, in press, 1992.
18. K. Stamnes, *J. Quant. Spectrosc. Radiat. Transfer* **28**, 47 (1982).
19. K. Stamnes, Ø. Lie-Svendsen, and M. H. Rees, *Planet. Space Sci.* **39**, 1435 (1991).